Applied Surface Science 610 (2023) 155437

Contents lists available at ScienceDirect

Applied Surface Science

journal homepage: www.elsevier.com/locate/apsusc

Full length article

The surface charge decay: A theoretical and experimental analysis

Mario Navarro-Rodriguez, Elisa Palacios-Lidon *, Andres M. Somoza *

Departamento de Fisica – CIOyN, Universidad de Murcia, Campus Espinardo, Murcia, 30100, Murcia, Spain

ARTICLE INFO

Keywords:
Surface charge
Surface conductivity
Charge decay rate
Surface potential decay
Kelvin Probe Force Microscopy

ABSTRACT

The ability to retain localized charges at the surface or interface of dielectric materials is a universal property that applies to many different fields such as tribocharging, charge nanopatterning, nanoxerography, etc. Once the surface is charged, its stability and subsequent discharging rate will determine the potential applications of a given system. This decay rate is properly defined by the macroscopic equations which depend on dielectric constants and conductivities of the two media. Here, we derive the equations to model the decay of charge distributions localized at the surface/interface of materials and solve them avoiding additional approximations made so far. Addressing the problem in the Fourier space, we arrive to a compact generic equation which provides a useful tool to determine both the bulk and surface conductivities of a material. Furthermore, we show that Kelvin Probe Force Microscopy (KPFM) is a particularly suited method to exploit this tool. Monitoring the charge decay of previously injected charge patches on silicon dioxide (SiO_2), together with an appropriated data analysis, we verify the behavior predicted by our equations. This allows us to characterize the surface and bulk conductivities of SiO_2 layers as well as its dependence with the relative humidity.

1. Introduction

It is well known that, specially in low-conductivity materials, surfaces may become charged. This charging process may be caused by tribocharging [1–3], deformation [4], contact with ionized gases [5–7], contact electrification [8–10] or corona discharge among others [11]. Independently of the origin of the surface charge distribution, its stability and temporal dissipation at the micro/nanoscale has been subjected to intense research due to its impact in modern technologies that rely on nanomaterial-based solutions [12–14]. For example, in polymeric [4,11,15,16] and ceramic [17,18] materials, controlled charge nanopatterns can be written with potential applications in high-density data storage, sensors, nanoxerography [19,20], energy harvesting [21,22], etc. Nanoscale charge patterning has been also used to study the charge dissipation along the dielectric blocking layer that prevents leakage currents in field-effect transistors [23–25].

The charge decay rate is determined mainly by the material conductivity and can be in the range of seconds to hours or even days or weeks. Moreover, the surface conductivity of a given material is usually heavily influenced by the environmental conditions [26], and in particular to the relative humidity (RH), due to adsorption of water vapor on the surface, [27] or due to ionic conduction [28,29]. Therefore understanding and quantifying the process of charge dissipation is crucial to characterize the conducting properties of new materials and to improve the performance of electronic devices.

Atomic Force Microscopy (AFM) related techniques such as Kelvin Probe Force Microscopy (KPFM) have been widely used to study charge dissipation in low conducting films due to its capability to detect localized charges with high sensitivity and nanoscale spatial resolution [30]. In addition, KPFM is a contactless, non-invasive technique that can be operated without the need for high source voltages. Moreover, the metallic tip can be also used to inject charge, enabling all-in-one experiments by recording the surface potential evolution of previously injected charges. Typically, the problem is analyzed through the spatial and temporal mapping of surface potentials (V_{KPFM}). Due to the absence of a reliable theory, usually the decay of the V_{KPFM} maximum is fitted to empirical laws, including exponential decay with one [31,32] or two characteristic times, [8,33–35] or to a stretched exponential [36,37].

However, an appropriate theory is necessary not only to characterize the time dependence of the problem but also to separate bulk and surface conduction and precisely define surface conductivity. Some authors have tried to construct such theory but resort to approximations to model the electric field inside the material [38,39]. Others, assume the same surface and bulk conductivity [40] or model the charge dissipation as a purely diffusive process, disregarding the effect of drift currents [1,28,29], etc. Furthermore, the role of the back electrode is under debate without a clear consensus about its contribution to the charge decay rate [8,16,41,42]. This highlights the importance of incorporating the correct geometry of the system into the equations.

* Corresponding authors.
E-mail addresses: elisapl@um.es (E. Palacios-Lidon), asg@um.es (A.M. Somoza).

https://doi.org/10.1016/j.apsusc.2022.155437
Received 31 August 2022; Received in revised form 10 October 2022; Accepted 21 October 2022
Available online 5 November 2022

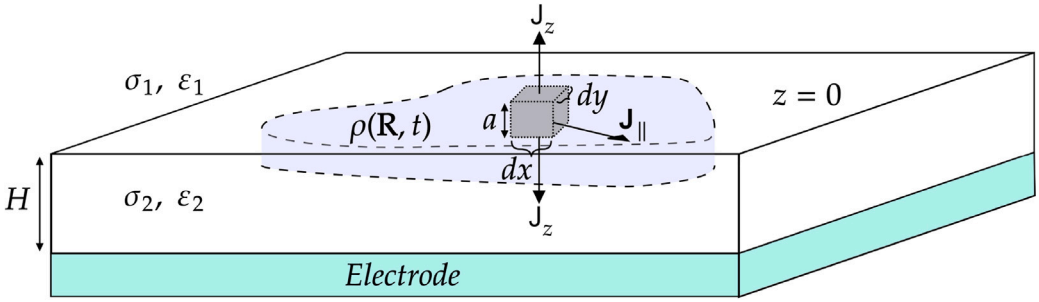

Fig. 1. Scheme of the modeled system.

In this work, we first derive the equations describing the generic problem of a charge distribution decaying at the interface between to media and through their solution we show the important role of the system geometry. Then, we show how our equations can be used to analyze the KPFM measurements, leading to a simple experimental method to quantitatively obtain both bulk and surface conductivities of a material as well as their dependence with external parameters.

2. Theory

It is well known that if a charge distribution, $\rho(\mathbf{R}, t = 0)$, is located inside a uniform, infinite and isotropic medium with conductivity σ and permittivity ε, the dissipation of such distribution through the bulk is governed by the equation (hereon, 2D vectors will be denoted with lowercase letters and uppercase letters will be used for 3D ones.)

$$\rho(\mathbf{R}, t) = \rho(\mathbf{R}, t = 0)e^{-t/\tau}, \tag{1}$$

where $\tau = \varepsilon/\sigma$ defines a characteristic timescale for charge dissipation. This straightforward result establishes that a bulk region without net charge in the initial state will remain neutral at any time. We emphasize that drift currents are the underlying mechanism for conduction. In most cases diffusion currents can be neglected because the charge gradients are minimal shortly after the dissipation process starts to take place [38].

To model the dissipation of an arbitrary charge distribution due to bulk and surface conduction we first consider the interface of two materials (set at $z = 0$), where the $z > 0$ half-space is filled by a medium with conductivity σ_1 and permittivity ε_1, while the $z < 0$ region corresponds to a medium with conductivity σ_2 and permittivity ε_2 of thickness H on top of a metallic back electrode (see Fig. 1). Then, a charge distribution, $\rho(\mathbf{R}, t = 0)$, of finite height, a, is located just inside the region $z < 0$. We assume that a is small enough to neglect any z dependence inside the elementary Gaussian surface defined by the cubic shaded region in Fig. 1.

Since a bulk region without net charge will remain neutral at any time, and because only drift currents are being considered, the different components of the current density are determined by Ohm's law,

$$\begin{aligned} \mathrm{J}_z(z > 0, \mathbf{r}) &= \sigma_1 \mathrm{E}_z, \\ \mathrm{J}_z(z < 0, \mathbf{r}) &= \sigma_2 \mathrm{E}_z, \\ \mathbf{J}_\parallel(-a < z < 0, \mathbf{r}) &= \sigma_\parallel \mathbf{E}_\parallel \end{aligned} \tag{2}$$

where different conductivities parallel and perpendicular to the interface ($\sigma_\parallel$ and σ_1, σ_2 respectively) are allowed. We note that σ_1, σ_2 and $\sigma_\parallel$ are defined as three-dimensional conductivities. Considering the continuity equation for the charge density,

$$a\frac{\partial \rho}{\partial t} = -\mathrm{J}_z(z = 0^+) + \mathrm{J}_z(z = -a) - a\nabla_\parallel \cdot \mathbf{J}_\parallel, \tag{3}$$

and applying Gauss's theorem,

$$\varepsilon_1 \mathrm{E}_z(z = 0^+) - \varepsilon_2 \mathrm{E}_z(z = -a) + a\varepsilon_2 \nabla_\parallel \cdot \mathbf{E}_\parallel = a\rho, \tag{4}$$

both $\mathbf{J}$ and $\mathbf{E}_\parallel$ can be eliminated from Eq. (3),

$$\begin{aligned} a\frac{\partial \rho}{\partial t} = &-\frac{\sigma_\parallel}{\varepsilon_2} a\rho + \left(\sigma_2 - \sigma_\parallel\right) \mathrm{E}_z(z = -a) \\ &- \left(\sigma_1 - \sigma_\parallel \frac{\varepsilon_1}{\varepsilon_2}\right) \mathrm{E}_z(z = 0^+). \end{aligned} \tag{5}$$

Similar equations to Eq. (5) have been previously derived although, as mentioned before, additional approximations were used [15,28,29,38–40,43]. Here we show that at this stage, the problem can be solved without any further approximations. In order to reach a closed equation for the surface charge density, $n(\mathbf{r}, t) = a\rho(\mathbf{R}, t)$, it is necessary to find the explicit form of the z component of the electric field. For that matter we solve the Poisson problem for a point charge located within the Gaussian surface. Since we are only interested in the evolution of the surface charge density, the potential at a given point in space is determined by

$$V(x, y, z) = \iint \mathrm{d}x'\mathrm{d}y'\; n(x', y') G(x - x', y - y', z, z' = z_0), \tag{6}$$

where the surface charge density is assumed to be located in a plane, $z' = z_0$, contained by the Gaussian surface shown in Fig. 1, and $G(x - x', y - y', z, z')$ is the Green function corresponding to the electrostatic potential generated at (x, y, z) due to the presence of a unit charge located at (x', y', z') [44]. Noting that $\mathrm{E}_z = -\partial V/\partial z$ and substituting into Eq. (5), one arrives to an integro-differential equation for $n(x, y, t)$. By taking its spatial 2D Fourier transform (FT) the equation is simplified to an ordinary differential equation (see Appendix A),

$$\begin{aligned} &\frac{\partial n(\mathbf{k}, t)}{\partial t} = -\frac{n(\mathbf{k}, t)}{\tau(k)}, \\ &n(\mathbf{k}, t) = n(\mathbf{k}, 0) \exp\left(-\frac{t}{\tau(k)}\right). \end{aligned} \tag{7}$$

where $n(\mathbf{k}, t)$ is the FT of the surface charge density, and $\tau(k)$ is determined by

$$\begin{aligned} \frac{1}{\tau(k)} = &\frac{\sigma_\parallel}{\varepsilon_2} - (\sigma_2 - \sigma_\parallel)\mathrm{E}_{1z}(k, z = -a, z' = z_0) + \\ &\left(\sigma_1 - \sigma_\parallel \frac{\varepsilon_1}{\varepsilon_2}\right) \mathrm{E}_{1z}(k, z = 0^+, z' = z_0). \end{aligned} \tag{8}$$

With $\mathrm{E}_{1z}(k, z)$ being the FT of the z component of the electric field generated by a single charge. In order to obtain the final equations, it is necessary to take the limit $a \to 0$. This allows to define a proper surface conductivity as $\sigma_s = \lim_{a \to 0} a\sigma_\parallel$ and to verify that the final equations do not depend on the microscopic details of the charge distribution (such as the shape of the Gaussian surface or the particular z_0 chosen).

2.1. Surface charge decay in a semi-infinite material

For the particularly simple case of a semi-infinite material ($H \to \infty$), where $\mathrm{E}_{1z}(k, t)$ is produced by a charge and a single image charge, $\tau(k)^{-1}$ is given by (see Appendix B)

$$\frac{1}{\tau(k)} = \frac{1}{\tau_0} + \frac{\sigma_s k}{\varepsilon_2 + \varepsilon_1}. \tag{9}$$

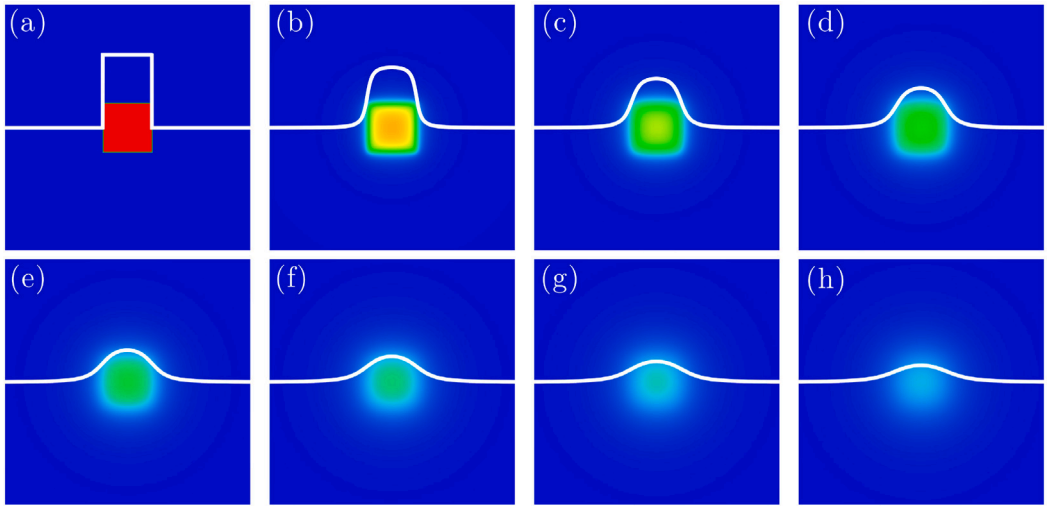

Fig. 2. (a)–(h) Charge decay evolution of an homogeneous square charge distribution. The delay time between successive frames is 40 s. Used parameters are $\sigma_1 = 0$, $\sigma_2 = 10^{-14}$ S/m, $\sigma_s = 10^{-21}$ S, $\varepsilon_1 = \varepsilon_0$, $\varepsilon_2 = 3.9\varepsilon_0$, $L_x = L_y = 50$ nm, Image size = 500×500 nm^2, $Q = 50\ e^-$.

with $\tau_0 \equiv \tau(k=0) = (\varepsilon_1 + \varepsilon_2)/(\sigma_1 + \sigma_2)$. In this case, the $k = 0$ mode corresponds to a relaxation process due to pure bulk conduction, which is equivalent to that of Eq. (1). Indeed, by setting $\varepsilon_1 = \varepsilon_2$ and $\sigma_1 = \sigma_2$ we recover the characteristic time of a charge embedded in a 3D-medium, $\tau = \varepsilon/\sigma$.

In the semi-infinite limit, the real space charge distribution, $n(\mathbf{r}, t)$, is obtained by performing the inverse FT of Eq. (7) with $\tau(k)$ given by Eq. (9),

$$n(\mathbf{r}, t) = \frac{e^{-t/\tau_0}}{2\pi} \int d\mathbf{r}' n(\mathbf{r}', 0) \frac{l(t)}{(l(t)^2 + |\mathbf{r} - \mathbf{r}'|^2)^{3/2}}, \tag{10}$$

where $l(t) = \sigma_s t/(\varepsilon_1 + \varepsilon_2)$. This integration can be performed for some simple geometries such as a rectangular homogeneous charge distribution of dimensions $(-L_x, L_x) \times (-L_y, L_y)$, commonly used in tribocharging patterning [1,29,45]. The analytical solution for this geometry is,

$$\begin{aligned} n(x, y, t) = \frac{Q e^{-t/\tau_0}}{8\pi L_x L_y} \Bigg[& \tan^{-1}\left(\frac{(L_x - x)(L_y - y)}{l(t)\sqrt{(L_x - x)^2 + (L_y - y)^2 + l(t)^2}} \right) + \\ & \tan^{-1}\left(\frac{(L_x + x)(L_y - y)}{l(t)\sqrt{(L_x + x)^2 + (L_y - y)^2 + l(t)^2}} \right) + \\ & \tan^{-1}\left(\frac{(L_x - x)(L_y + y)}{l(t)\sqrt{(L_x - x)^2 + (L_y + y)^2 + l(t)^2}} \right) + \\ & \tan^{-1}\left(\frac{(L_x + x)(L_y + y)}{l(t)\sqrt{(L_x + x)^2 + (L_y + y)^2 + l(t)^2}} \right) \Bigg]. \end{aligned} \tag{11}$$

A particular example of the time evolution of a square charge distribution localized at the surface of a material is shown in Fig. 2. We note that for long times the shape of the charge distribution becomes circular. Recently, it was suggested that this shape evolution could be due to pure diffusion [29], but our results show that drift currents produce the same effect and seems like a more plausible cause as explained later on.

Moreover, it can be proved that near the center of a charge domain, in the long-time limit, the charge distribution decays as

$$n(\mathbf{0}, t) = \frac{Q}{2\pi l(t)^2} e^{-t/\tau_0} + \mathcal{O}(e^{-t/\tau_0}/t^4), \tag{12}$$

with Q being the total charge. This expression allows for the direct estimation of τ_0, while to obtain the surface conductivity, included in $l(t)$, the total initial charge must be known.

2.2. Surface charge decay in a thin film

For thin films, the semi-infinite approximation is not adequate and the effect of the back electrode located at $z = -H$ will change $\tau(k)$. This problem is analytically solved finding that (see Appendix C)

$$\frac{1}{\tau(k)} = \frac{\sigma_2 \cosh(kH) + (\sigma_1 + k\sigma_s) \sinh(kH)}{\varepsilon_2 \cosh(kH) + \varepsilon_1 \sinh(kH)} \tag{13}$$

It is worth noting that in spite of a more complex k dependence than in the semi-infinite case, $\tau(k)^{-1}$ remains linear with respect to σ_1, σ_2 and σ_s. Eqs. (7) and (13) constitute an important result: in contrast with the charge decay in a 3D medium, where only one characteristic time can be defined, now each Fourier mode dissipates with its own characteristic time. The existence of a continuum of $\tau(k)$ is a consequence of separating surface and bulk conduction (as easily seen in the semi-infinite case) as well as to the presence of the back electrode at a finite distance. This result sheds light on the controversy of the role played by the back electrode, some authors report that the decay time increases with the distance to the back electrode [16] while others claim the opposite [8,41,42]. Our equations show that the role of the electrode depends not only on ε_1, ε_2 and σ_1, σ_2 and σ_s of the materials but also on the kH value. While H is fixed for a given system, the effective value of k that must be considered depends on the scale of observation. Hence, different behaviors varying H can be consistent.

At this point, we recall that we have only considered drift currents neglecting diffusion ones as they are minimal in many cases. However, we note that including a two-dimensional diffusion current term, $-D\nabla_{\parallel} n(\mathbf{r}, t)$ would not modify Eq. (7) and such process can be easily incorporated adding a term Dk^2 to Eq. (8). However, we note that in many thin film-based experiments, the scale of observation is of the order of microns while the film thickness may vary from few to hundreds of nanometers. In this situation $kH \ll 1$ and Eq. (13) can be expanded in powers of kH

$$\frac{1}{\tau(k)} = \frac{\sigma_2}{\varepsilon_2} + \frac{\varepsilon_2\sigma_1 - \varepsilon_1\sigma_2}{\varepsilon_2^2} k + \frac{H^2(\varepsilon_1^2\sigma_2 - \varepsilon_1\varepsilon_2\sigma_1) + H\varepsilon_2^2\sigma_s}{\varepsilon_2^3} k^2 + O((kH)^3). \tag{14}$$

Additionally, in the case that bulk conductivity in both media is very small, in particular, $\sigma_1, \sigma_2 \ll \sigma_s$, Eq. (14) resembles a diffusion equation

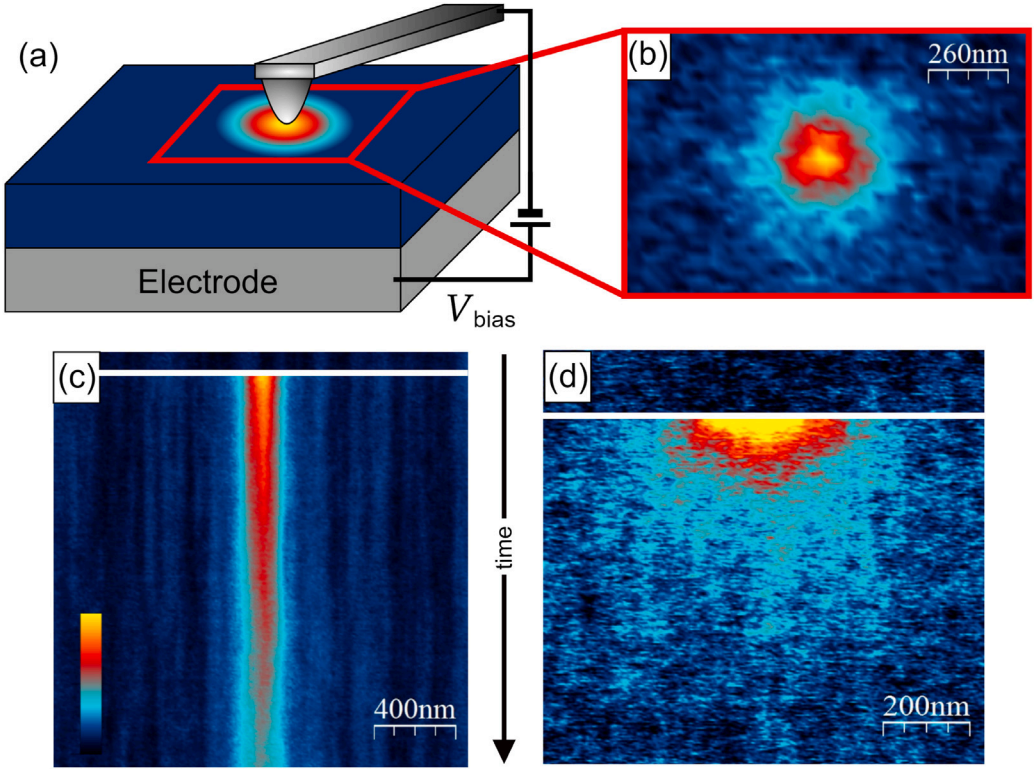

Fig. 3. (a) Diagram of the charge injection procedure. (b) V_{KPFM} image of an injected positive charge. (c) and (d) V_{KPFM} charge decay experiments performed at 14% and 28% RH respectively. As explained in the main text, the vertical axis is time. The horizontal white line indicates the moment when the charge is injected. Line scan frequency is 0.501 Hz and $\Delta z = 1.3$ V in all the images.

with an effective diffusion constant $D \approx H\sigma_s/\varepsilon_2$. As mentioned in the previous subsection, in [29] it was shown that the discharging experimental results could be well fitted to a purely diffusive process. It would be interesting to clarify in the future whether the dominant transport process corresponds to diffusion or drift currents.

3. Results and discussion

Eq. (13) provides a direct procedure to determine σ_1, σ_2 and σ_s from the fit of the measured $\tau(k)$. Experimentally, it can be implemented using KPFM techniques, since for surface charge distributions the FT of the measured KPFM voltage is directly proportional to $n(\mathbf{k}, t)$ [46]. To corroborate the validity of our equations, we have carried out charge decay experiments on a SiO_2 film thermally grown on highly doped p-type silicon. Besides its obvious technological interest for the fabrication of electronic devices, SiO_2 on silicon provides a suitable platform to validate the proposed equations. The surface conductivity of SiO_2 is much more sensitive to small RH changes than the bulk one because the surface conductivity heavily depends on the amount of adsorbed water molecules [27,47,48]. Thus, a slight variation of RH changes the amount of physisorbed molecules and therefore we can tune the surface conductivity while keeping the bulk one mostly constant.

3.1. Materials and methods

We have used a 300 nm thick SiO_2 film thermally grown on (100) p-type silicon (1–10 Ω cm, Siltronix). The surface was cleaned with ethanol, rinsed with double distilled water and then placed on a heating plate at 65 °C for several hours in order to remove the physisorbed water. The Experiments were carried out at room temperature and controlled humidity in a N_2 atmosphere. In order to allow the humidity to stabilize we let the system at a given humidity for at least one hour. Circular charge patches were injected into the SiO_2 layer by means of contact electrification: tip and sample were brought into contact while applying a bias voltage (4–6 V) during about 40 ms. Similar positive or negative charge patches are obtained by changing the sign of the bias voltage pulse (Fig. 3(a)). The amount and size of the charge is controlled by adjusting the intensity as well as the applied loading force [49]. Just after the charge is injected, its decay is monitored by means of Frequency Modulation-KPFM (FM-KPFM). Taking advantage of the radial symmetry of the charge (Fig. 3(b)), instead of acquiring successive $x - y$ images, we kept the y-scan position fixed while the x direction is scanned repeatedly (Fig. 3(c), (d)). This allows to reach medium acquisition data rates and helps minimizing the tip-induced contribution to the charge dissipation [16,18,50]. A Nanotec SFM system with a PLL/dynamic measurement board was used along with Pt-coated tips (OMCL-AC240TM-R3, k = 2–4 N/m). To improve the lateral resolution and to minimize the tip induced effects, topography feedback was operated in frequency modulation non-contact dynamic mode (FM-DSFM) with an oscillation amplitude of 1 nm and tip-sample distances of 5–10 nm. The V_{KPFM} images were obtained using FM-KPFM mode with V_{AC} = 500 mV at ν_{AC} = 7 kHz [51].

3.2. Experimental results

Fig. 3(c) and (d) show two experiments performed at different RHs (14% and 28% respectively). A first look already evidences a stark charge decay dependence on the RH, being faster for higher RH. Moreover, at lower RH the charge barely spreads over the surface, indicating that the charge is mainly dissipated through the bulk, while at higher RH the surface conductivity plays a greater role spreading the charge.

The V_{KPFM} images acquired for a injection–dissipation experiment are processed by calculating the Fast Fourier Transform (FFT) of each x-scan line to obtain the $V_{KPFM}(k_n, t_i)$ image (Fig. 4(a)). The time

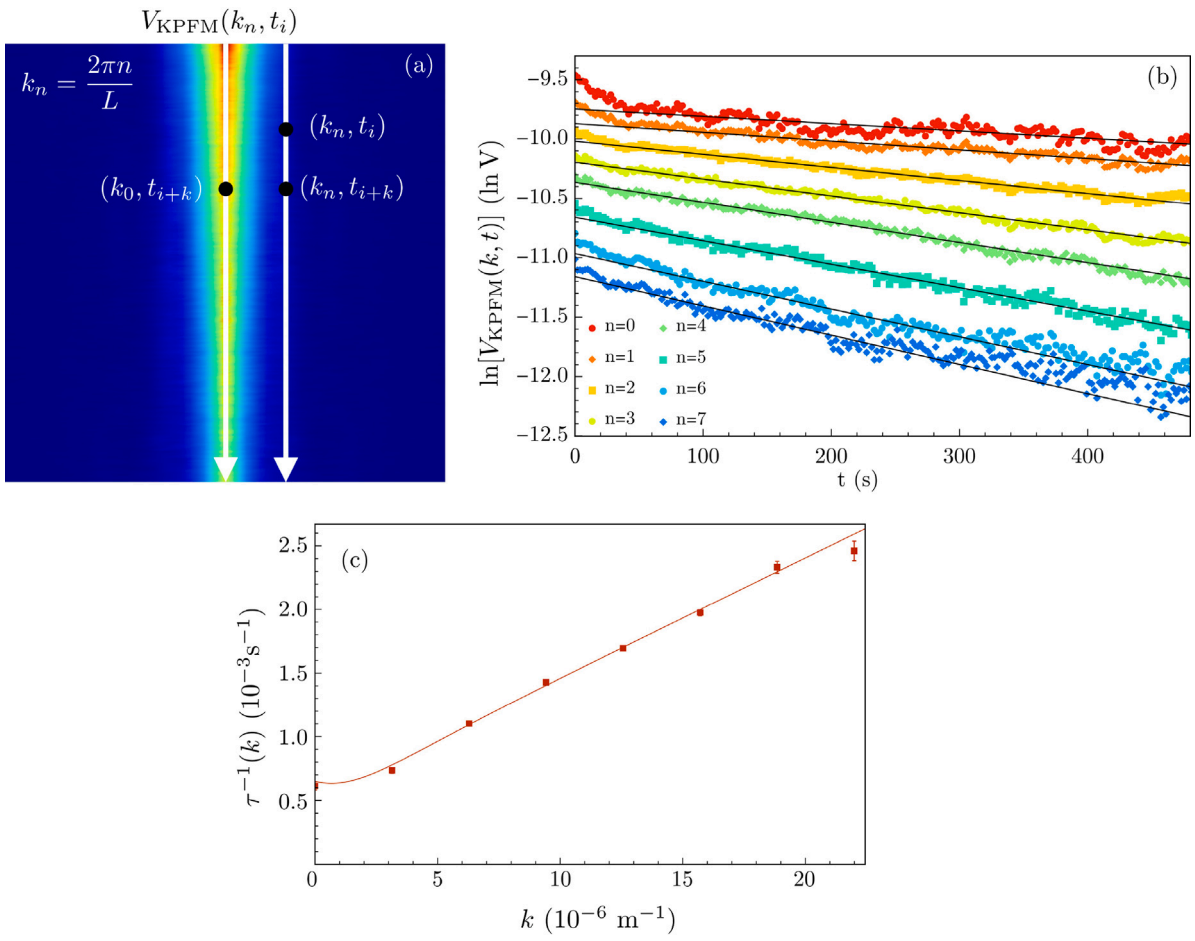

Fig. 4. (a) $V_{\mathrm{KPFM}}(k_n, t_i)$ image corresponding to Fig. 3(c). (b) Time evolution of different k_n (RH = 14%) together with their corresponding fit (solid lines) to Eq. (7). Each n corresponds to a Fourier mode with $k_n = 2\pi n/L$, with L being the image size. (c) $\tau(k_n)^{-1}$ vs. k plot. The solid line corresponds to the fit to Eq. (13).

evolution of each Fourier mode (k_n) is then obtained from the vertical profiles (white solid vertical line in Fig. 4(a)). Fig. 4(b) shows the time evolution of some Fourier modes, the data shows an excellent linear behavior that verifies the main predictions of our equations: (1) an exponential decay of the $V_{\mathrm{KPFM}}(k = k_n, t)$ signal and (2) a k-dependent decay time. The characteristic time, $\tau(k_n)$, is estimated by fitting each profile to Eq. (7). We note that the decay rate shortly after injection deviates from the linear behavior. We appreciate two possible reasons: (*i*) when the surface charge is large the tip might produce a non negligible electrostatic interaction, and (*ii*) the FFT assumes that all the points of a given profile are measured simultaneously, while in reality the first and last point of each horizontal profile differ by two seconds in our particular case. It is also worth mentioning that when a given Fourier mode has decayed almost completely the signal starts to be dominated by the noise (as in the last dark blue points in Fig. 4(b)) and must be excluded from the fit. Finally, for a given experiment we plotted $\tau(k_n)^{-1}$ versus k_n and we fitted this data to Eq. (13) to estimate both bulk and surface conductivities of SiO_2 as shown in Fig. 4(c). For the fit we have assumed $\sigma_1 = 0$, $\varepsilon_1 = \varepsilon_0$, $\varepsilon_{SiO_2} = 3.9\varepsilon_0$ and $H = 300$ nm, being σ_2 and σ_s the only free parameters.

This procedure is carried out at different RHs, as shown in Fig. 5. The corresponding σ_2 and σ_s for each RH are listed in Table 1.

We observe that the bulk conductivity slightly varies in the RH range of our experiments, although a small increase is found at higher RH. This increase may be due to water molecules diffusing through the volume. Although the 300 nm SiO2 growth on Si by wet thermal oxidation is expected to have high quality and low porosity, and the humidity rage used in our experiments is relatively low, we cannot discard that some water spreads over the bulk, increasing the conductivity. Actually, we see that the main bulk and surface conductivity increases are correlated and take place at RH just above 10% (after that, the bulk conductivity remains mostly constant). If there is more water at the surface the probability that it diffuses through the volume is also higher. In any case, our values still remain in good agreement with those reported in the literature under similar conditions [52]. SiO_2's surface conductivity varies more than one order of magnitude in the same RH range, which is to be expected since σ_s strongly depends on the surface treatment, cleaning procedure as well as on the ambient conditions. Thus, a direct comparison with previously reported values is not straightforward. However, σ_s values between 10^{-21} S and 10^{-22} S, such as those shown in Table 1 are compatible with estimations obtained from models accounting for physisorbed water on the surface [27].

Table 1
Bulk and surface conductivities obtained from the fits of Fig. 5 at different RHs.

RH (%)	σ_2 (10^{-14} S/m)	σ_s (10^{-22} S)
10	1.53 ± 0.10	4.8 ± 1.6
14	2.24 ± 0.12	40.9 ± 1.3
16	2.40 ± 0.22	61.5 ± 1.7
18	2.43 ± 0.12	75.3 ± 1.3

4. Conclusions

In conclusion, we have derived the appropriate equations for the surface charge decay in homogeneous media. This system presents

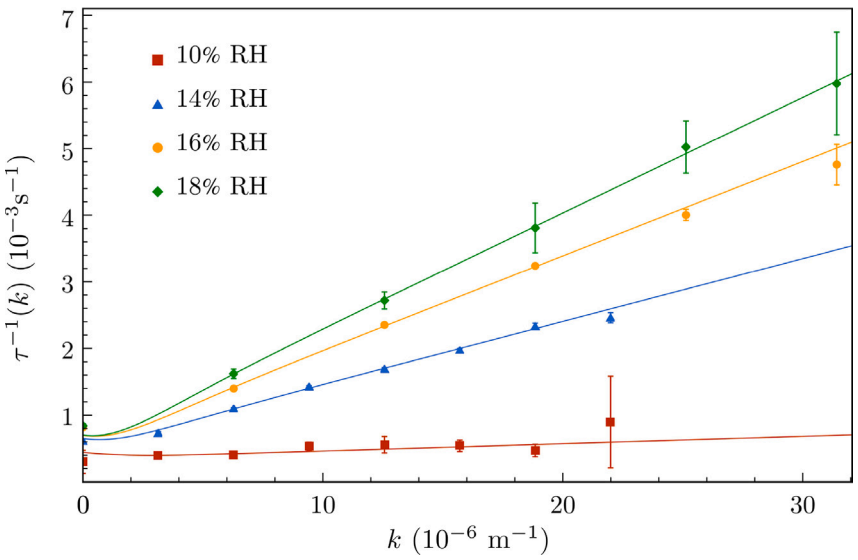

Fig. 5. τ^{-1} vs. k plot obtained from experiments performed at different RHs. Solid lines correspond to the fit to Eq. (13).

multiple decay times that are well defined in Fourier space. We have exactly solved the equations for the standard and widely used geometry of a film on top of a back electrode. When both bulk and surface conduction are comparable, the availability of the exact equations is particularly important because the decay times depend on the geometry of the system (in particular on the film thickness, H). An inaccurate treatment could lead to the wrong conclusion that surface and bulk conductivities depend on H.

We have also proposed a new experimental method based on standard KPFM measurements to quantitatively determine both bulk and surface conductivities. Since the KPFM signal can be directly Fourier transformed, these measurements allow for the direct verification of the exponential decay of each Fourier mode. The fitting of the relaxation time for each Fourier mode provides a simple and sensitive procedure to estimate surface and bulk conductivity, especially for highly insulating systems. We note that similar KPFM measurements have been performed in many different systems and our model could help to reinterpret previous experiments. We hope that our theoretical analysis clarifies the surface charge decay problem which is of broad interest and that the proposed experimental method helps to shed light about the electronic properties of new low-conducting materials.

CRediT authorship contribution statement

Mario Navarro-Rodriguez: Investigation, Data curation, Visualization, Writing – review & editing. **Elisa Palacios-Lidon:** Conceptualization, Methodology, Supervision, Writing – original draft, Funding acquisition. **Andres M. Somoza:** Methodology, Formal analysis, Writing – review & editing, Funding acquisition.

Declaration of competing interest

The authors declare that they have no known competing financial interests or personal relationships that could have appeared to influence the work reported in this paper.

Funding

This research was supported by MCIN/AEI/10.13039/501100011033/ through the project PID2019-104272RB-C52, by "ERDF A way of making Europe" and the Fundación Séneca, Spain through the project 20860/PI/18. M.N work was financed by the grant PID2019-104272RB-C52/PRE2020-094503 funded by MCIN/AEI/10.13039/501100011033 and by "ESF Investing in your future".

Data availability

Data will be made available on request.

Appendix A. Simplification of the equation for the surface charge

We assume that all the charge is located in the plane $z' = z_0 < 0$. Then, by substituting the Green function in the expression for the potential, Eq. (6), and noting that $\mathrm{E}_z = -\partial V/\partial z$,

$$\begin{aligned}\mathrm{E}_z &= -\iint \mathrm{d}x'\ \mathrm{d}y'\ n(x',y')\frac{\partial G(x-x',y-y',z,z')}{\partial z}\\ &= \iint \mathrm{d}x'\ \mathrm{d}y'\ n(x',y')\mathrm{E}_{1z}(x-x',y-y',z,z').\end{aligned} \tag{A.1}$$

with E_{1z} being the electric field generated by a single point charge (and its associated image charges). Substituting (A.1) into Eq. (5) from the main text, and noting that $n(x,y) \equiv a\rho(\mathbf{R},t)$, we have

$$\begin{aligned}\frac{\partial n(x,y)}{\partial t} = &-\frac{\sigma_\parallel}{\varepsilon_2}n(x,y) + (\sigma_2-\sigma_\parallel)\iint \mathrm{d}x'\ \mathrm{d}y'\ n(x',y')\\ &\times \mathrm{E}_{1z}(x-x',y-y',-a,z')\\ &-\left(\sigma_1-\sigma_\parallel\frac{\varepsilon_1}{\varepsilon_2}\right)\iint \mathrm{d}x'\ \mathrm{d}y'\ n(x',y')\\ &\times \mathrm{E}_{1z}(x-x',y-y',0^+,z').\end{aligned} \tag{A.2}$$

Thus, we have arrived to a closed integro-differential equation for the surface charge density, $n(x,y)$. This seemingly daunting equation is simplified by taking its spatial Fourier Transform (FT),

$$\begin{aligned}\frac{\partial n(\mathbf{k},t)}{\partial t} = &-\frac{\sigma_\parallel}{\varepsilon_2}n(\mathbf{k},t) + (\sigma_2-\sigma_\parallel)\, n(\mathbf{k},t)\mathrm{E}_{1z}(\mathbf{k},-a,z')\\ &-\left(\sigma_1-\sigma_\parallel\frac{\varepsilon_1}{\varepsilon_2}\right)n(\mathbf{k},t)\mathrm{E}_{1z}(\mathbf{k},0^+,z').\end{aligned} \tag{A.3}$$

The functions with the argument $\mathbf{k}$ are the 2D FT of their respective real space counterparts. Since the electric field generated by a point charge has radial symmetry it will only depend on $k = |\,\mathbf{k}\,|$. We define

$$\frac{1}{\tau(k)} = \frac{\sigma_\parallel}{\varepsilon_2} - (\sigma_2-\sigma_\parallel)\mathrm{E}_{1z}(k,z=-a,z') + \left(\sigma_1-\sigma_\parallel\frac{\varepsilon_0}{\varepsilon}\right)\mathrm{E}_{1z}(k,z=0^+,z'), \tag{A.4}$$

which allows the equation in the Fourier space to be simplified to

$$\frac{\partial n(\mathbf{k},t)}{\partial t} = -\frac{n(\mathbf{k},t)}{\tau(k)}, \qquad n(\mathbf{k},t) = n(\mathbf{k},0)e^{-t/\tau(k)}, \tag{A.5}$$

where $\tau(k)$ is the characteristic time for charge dissipation in the Fourier space. In order to particularize this equation, the FT of the electric field generated by one charge has to be specified.

Appendix B. Electric field in the semi-infinite case

We consider dielectric constant ε_1 and bulk conductivity σ_1 for $z > 0$ and ε_2 and σ_2 for $z < 0$. The Green function of a point charge located at (x', y', z') inside the region $-a < z' < 0$, is obtained by adding the potential generated by the original point charge and its corresponding image. In the region $z < 0$ and for $z' < 0$, we have

$$G(x-x', y-y', z, z') = \frac{1}{4\pi\varepsilon_2\sqrt{|\mathbf{r}-\mathbf{r}'|^2+|z-z'|^2}} + \frac{s}{4\pi\varepsilon_2\sqrt{|\mathbf{r}-\mathbf{r}'|^2+|z+z'|^2}}, \tag{B.1}$$

where $s = (\varepsilon_2 - \varepsilon_1)/(\varepsilon_2 + \varepsilon_1)$. Making use of the expression

$$\frac{1}{\sqrt{r^2+|z-z'|^2}} = \int_0^\infty \mathrm{d}m\, J_0(rm) e^{-m|z-z'|}, \tag{B.2}$$

and applying the procedure described below, through Eqs. (C.3)–(C.5), it is easy to directly calculate de FT of $E_{1z}(|\mathbf{r}-\mathbf{r}'|, z, z')$. For a unit charge located at $(0, 0, z')$, we obtain:

$$\mathrm{E}_{1z}(k, z, z') = \frac{(z-z')e^{-k|z-z'|}}{2\varepsilon_2|z-z'|} - \frac{s e^{k(z+z')}}{2\varepsilon_2}. \tag{B.3}$$

We emphasize that since our image charge is located in the $z > 0$ region, this expression is valid only when $z < 0$ and $z' < 0$. The electric field in the $z > 0$ region is obtained by imposing the continuity of the electric field at the interface between the two regions,

$$\varepsilon_1 E_{1z}(k, 0^+, z') = \varepsilon_2 E_{1z}(k, 0^-, z'). \tag{B.4}$$

Substituting Eq. (B.3) in Eq. (8) and taking the limit $a \to 0$, we find that in the semi-infinite case $\tau(k)^{-1}$ takes the form

$$\frac{1}{\tau(k)} = \frac{\sigma_2+\sigma_1}{\varepsilon_2+\varepsilon_1} + \frac{\sigma_s k}{\varepsilon_2+\varepsilon_1}. \tag{B.5}$$

We recall that $\lim_{a\to 0} a\sigma_\parallel = \sigma_s$, but $\lim_{a\to 0} a\sigma_1 = \lim_{a\to 0} a\sigma_2 = 0$.

Appendix C. Electric field in the presence of a back electrode at $z = -H$

We consider the same geometry as in the main text, where the $z > 0$ half space is filled by a medium with conductivity σ_1 and permittivity ε_1 (region a). The region $0 < z < -H$ (region b) is filled by a medium with conductivity σ_2 and permittivity ε_2. The back electrode occupies the $z < -H$ region (region c). As such, for a charge located at ($\mathbf{r}' = 0, z' = z_0$) with $-H < z_0 < 0$, the potential in each region can be written as

$$\begin{aligned} V_{1,a}(r, z, z') &= \frac{q}{4\pi\varepsilon_1}\int_0^\infty \mathrm{d}m\, J_0(rm) A(m) e^{-mz} && z > 0, \\ V_{1,b}(r, z, z') &= \frac{q}{4\pi\varepsilon_1}\int_0^\infty \mathrm{d}m\, J_0(rm) \\ &\quad \times \left(\frac{\varepsilon_1}{\varepsilon_2} e^{-m|z-z_0|} + B(m)e^{-mz} + C(m)e^{mz}\right) && -H < z < 0. \end{aligned} \tag{C.1}$$

In order to find the expressions for $A(m)$, $B(m)$, and $C(m)$ we apply the boundary conditions for the electric potential and its normal derivatives at each interface,

$$\begin{aligned} &V_{1,a}(r, z=0^+, z') = V_{1,b}(r, z=0^-, z'), \quad \varepsilon_1 \frac{\mathrm{d}V_{1,a}}{\mathrm{d}z}\Big|_{z=0^+} = \varepsilon_2 \frac{\mathrm{d}V_{1,b}}{\mathrm{d}z}\Big|_{z=0^-} \\ &V_{1,b}(r, z=-H^+, z') = 0. \end{aligned} \tag{C.2}$$

Since we are interested on the FT of the z component of the electric field, $\mathrm{E}_{1z}(k, z, z')$, we calculate the FT of each of these potentials. As every integral of Eq. (C.1) has the same functional form,

$$V_{1,i}(r, z, z') = \int_0^\infty \mathrm{d}m J_0(rm) f_i(m, z, z'), \tag{C.3}$$

their FT is given by

$$\begin{aligned} V_{1,i}(k, z, z') &= \int_0^\infty \mathrm{d}m \int \mathrm{d}^2 r J_0(rm) f_i(m, z, z') e^{-i\mathbf{k}\cdot\mathbf{r}} \\ &= \int_0^\infty \mathrm{d}m \int_0^\infty \mathrm{d}r \int_0^{2\pi} \mathrm{d}\theta\; r J_0 f_i(m, z, z') e^{-ikr\cos(\theta)} \\ &= 2\pi \int_0^\infty \mathrm{d}m\; f_i(m, z, z') \underbrace{\int_0^\infty \mathrm{d}r\; r J_0(rm) J_0(km)}_{\delta(k-m)/m} \\ &= 2\pi \frac{f_i(k, z, z')}{k}. \end{aligned} \tag{C.4}$$

where $f_i(k, z, z')$ is the original function but with the argument k instead of m. Then, $\mathrm{E}_{1z}(k, z, z')$ is obtained by computing

$$\mathrm{E}_{1z,i}(k, z, z') = -\frac{2\pi}{k}\frac{\partial f_i(k, z, z')}{\partial z}. \tag{C.5}$$

The explicit equations for $z > 0$ and $z < 0$ are given by

$$\begin{aligned} \mathrm{E}_{1z,a}(k, z > 0, z') &= \frac{e^{-k(z+z_0)}(e^{2k(H+z')} - 1)}{(\varepsilon_2-\varepsilon_1) + e^{2Hk}(\varepsilon_1+\varepsilon_2)}, \\ \mathrm{E}_{1z,b}(k, -H < z < 0, z') &= \frac{1}{2\varepsilon_2}\left(\frac{e^{k(z-z')}(e^{2k(H+z')}-1)(\varepsilon_1-\varepsilon_2)}{(\varepsilon_2-\varepsilon_1)+e^{2Hk}(\varepsilon_1+\varepsilon_2)}\right. \\ &\quad + \frac{e^{-k(H+z)}(\varepsilon_1\sinh(kz') - \varepsilon_2\cosh(kz'))}{\varepsilon_2\cosh(kH) - \varepsilon_1\sinh(kH)} \\ &\quad \left. + e^{-k|z-z'|}\frac{(z-z')}{|z-z'|}\right). \end{aligned} \tag{C.6}$$

These expressions allow for the calculation of $\mathrm{E}_{1z}(k, 0^+, z')$, and $\mathrm{E}_{1z}(k, -a, z')$. Substituting these expressions into Eq. (8) and taking the limit $a \to 0$ we find the expression for $\tau(k)$:

$$\frac{1}{\tau(k)} = \frac{\sigma_2\cosh(kH) + (\sigma_1 + k\sigma_s)\sinh(kH)}{\varepsilon_2\cosh(kH) + \varepsilon_1\sinh(kH)}. \tag{C.7}$$

References

[1] Y.S. Zhou, Y. Liu, G. Zhu, Z.-H. Lin, C. Pan, Q. Jing, Z.L. Wang, In Situ Quantitative Study of Nanoscale Triboelectrification and Patterning, Nano Lett. 13 (6) (2013) 2771–2776, http://dx.doi.org/10.1021/nl401006x.

[2] H.T. Baytekin, A.Z. Patashinski, M. Branicki, B. Baytekin, S. Soh, B.A. Grzybowski, The Mosaic of Surface Charge in Contact Electrification, Science 333 (6040) (2011) 308–312, http://dx.doi.org/10.1126/science.1201512.

[3] B. Shi, X. Gan, C. Zhang, H. Lang, K. Zou, T. Bu, Y. Peng, Investigating the effect of nanoscale triboelectrification on nanofriction in insulators, Nano Energy 91 (2022) 106620, http://dx.doi.org/10.1016/j.nanoen.2021.106620.

[4] Q. Li, A. Peer, I.H. Cho, R. Biswas, J. Kim, Replica molding-based nanopatterning of tribocharge on elastomer with application to electrohydrodynamic nanolithography, Nature Commun. 9 (1) (2018) 974, http://dx.doi.org/10.1038/s41467-018-03319-4.

[5] A.M. Welle, H.O. Jacobs, Printing of organic and inorganic nanomaterials using electrospray ionization and Coulomb-force-directed assembly, Appl. Phys. Lett. 87 (26) (2005) 263119, http://dx.doi.org/10.1063/1.2149985.

[6] A. Hong, S.J. Lee, C.M. Choi, J.Y. Baek, M.C. Choi, Neutral gas effect on the surface potential and charge compensation of an insulating sample, Appl. Surf. Sci. 572 (2022) 151338, http://dx.doi.org/10.1016/j.apsusc.2021.151338.

[7] S.J. Lee, A. Hong, I.H. Kim, C.M. Choi, B.K. Min, J.Y. Baek, M.C. Choi, Surface potential measurements of a polymer film following primary ion gun irradiation for ToF-SIMS analysis of insulator using a Kelvin probe and the observation of effects from the vacuum gauge, Appl. Surf. Sci. 525 (2020) 146561, http://dx.doi.org/10.1016/j.apsusc.2020.146561.

[8] N. Felidj, J. Lambert, C. Guthmann, M.S. Jean, Charge stability on thin insulators studied by atomic force microscopy, EPJ Appl. Phys. 12 (2) (2000) 85–91, http://dx.doi.org/10.1051/epjap:2000174.

[9] J. Wang, H. Zhang, G.-s. Cao, L.-h. Xie, W. Huang, Injection and Retention Characterization of Trapped Charges in Electret Films by Electrostatic Force Microscopy and Kelvin Probe Force Microscopy, Phys. Status Solidi A 217 (20) (2020) http://dx.doi.org/10.1002/pssa.202000190.

[10] K. Shi, B. Chai, H. Zou, D. Min, S. Li, P. Jiang, X. Huang, Dielectric Manipulated Charge Dynamics in Contact Electrification, Research 2022 (2022) http://dx.doi.org/10.34133/2022/9862980.

[11] X. Li, Y. Wang, M. Xu, Y. Shi, H. Wang, X. Yang, H. Ying, Q. Zhang, Polymer electrets and their applications, J. Appl. Polym. Sci. 138 (19) (2021) 50406, http://dx.doi.org/10.1002/app.50406.

[12] H.O. Jacobs, G.M. Whitesides, Submicrometer Patterning of Charge in Thin-Film Electrets, Science 291 (5509) (2001) 1763–1766, http://dx.doi.org/10.1126/science.1057061.

[13] M.G. Ji, Q. Li, R. Biswas, J. Kim, Stability and temporal decay of nanopatterned tribocharge on nanotextured elastomer surfaces, Nano Energy 79 (2021) 105441, http://dx.doi.org/10.1016/j.nanoen.2020.105441.

[14] S. Gödrich, H.-W. Schmidt, G. Papastavrou, Stability of Charge Distributions in Electret Films on the nm-Scale, ACS Appl. Mater. Interfaces 14 (3) (2022) 4500–4509, http://dx.doi.org/10.1021/acsami.1c21174.

[15] D. Zhao, L. Duan, M. Xue, W. Ni, T. Cao, Patterning of Electrostatic Charge on Electrets Using Hot Microcontact Printing, Angew. Chem. Int. Ed. 48 (36) (2009) 6699–6703, http://dx.doi.org/10.1002/anie.200902627.

[16] N. Knorr, S. Rosselli, G. Nelles, Surface-potential decay of biased-probe contact-charged amorphous polymer films, J.S 107 (5) (2010) 054106, http://dx.doi.org/10.1063/1.3309763.

[17] R. Alvarado, L. Karam, R. Dahmani, A. Lepicard, F. Calzavara, A. Piarristeguy, A. Pradel, T. Cardinal, F. Adamietz, E. Fargin, M. Chazot, K. Richardson, L. Vellutini, M. Dussauze, Patterning of the Surface Electrical Potential on Chalcogenide Glasses by a Thermoelectrical Imprinting Process, J. Phys. Chem. C 124 (42) (2020) 23150–23157, http://dx.doi.org/10.1021/acs.jpcc.0c06507.

[18] T.J. Moran, K. Suzuki, T. Hosokura, A. Khaetskii, B.D. Huey, Charge injection and decay of nanoscale dielectric films resolved via dynamic scanning probe microscopy, J. Am. Ceram. Soc. 104 (10) (2021) 5157–5167, http://dx.doi.org/10.1111/jace.17776.

[19] H. Jacobs, S. Campbell, M. Steward, Approaching Nanoxerography: The Use of Electrostatic Forces to Position Nanoparticles with 100 nm Scale Resolution, Adv. Mater. 14 (21) (2002) 1553–1557, http://dx.doi.org/10.1002/1521-4095(20021104)14:21<1553::AID-ADMA1553>3.0.CO;2-9.

[20] E. Palleau, L. Ressier, Combinatorial Particle Patterning by Nanoxerography, Adv. Funct. Mater. 28 (30) (2018) 1801075, http://dx.doi.org/10.1002/adfm.201801075.

[21] V. Slabov, S. Kopyl, M.P. Soares dos Santos, A.L. Kholkin, Natural and Eco-Friendly Materials for Triboelectric Energy Harvesting, Nano-Micro Lett. 12 (1) (2020) 42, http://dx.doi.org/10.1007/s40820-020-0373-y.

[22] S. Devasahayam, C.M. Hussain, Nano Tools and Devices for Enhanced Renewable Energy, Elsevier, 2021.

[23] K. Makasheva, C. Villeneuve-Faure, C. Bonafos, C. Laurent, A. Pugliara, B. Despax, L. Boudou, G. Teyssedre, Dielectric Engineering of Nanostructured Layers to Control the Transport of Injected Charges in Thin Dielectrics, IEEE Trans. Nanotechnol. 15 (6) (2016) 839–848, http://dx.doi.org/10.1109/TNANO.2016.2553179.

[24] R. Castagne, P. Hesto, A. Vapaille, Surface conductivity of the insulator of an MIS or MIM device, Thin Solid Films 17 (3) (1973) 253–264, http://dx.doi.org/10.1016/0040-6090(73)90134-X.

[25] U. Zaghloul, G.J. Papaioannou, B. Bhushan, F. Coccetti, P. Pons, R. Plana, New insights into reliability of electrostatic capacitive RF MEMS switches, Int. J. Microw. Wirel. Technol. 3 (5) (2011) 571–586, http://dx.doi.org/10.1017/S1759078711000766.

[26] C. Heinert, R.M. Sankaran, D.J. Lacks, Decay of electrostatic charge on surfaces due solely to gas phase interactions, J. Electrostat. 115 (2022) http://dx.doi.org/10.1016/j.elstat.2021.103663.

[27] J.A. Voorthuyzen, K. Keskin, P. Bergveld, Investigations of the surface conductivity of silicon dioxide and methods to reduce it, Surf. Sci. 187 (1) (1987) 201–211, http://dx.doi.org/10.1016/S0039-6028(87)80132-2.

[28] M. Konený, M. Bartošík, J. Mach, V. varc, D. Nezval, J. Piastek, P. Procházka, A. Cahlík, T. ikola, Kelvin Probe Force Microscopy and Calculation of Charge Transport in a Graphene/Silicon Dioxide System at Different Relative Humidity, ACS Appl. Mater. Interfaces 10 (14) (2018) 11987–11994, http://dx.doi.org/10.1021/acsami.7b18041.

[29] X. Bai, A. Riet, S. Xu, D.J. Lacks, H. Wang, Experimental and Simulation Investigation of the Nanoscale Charge Diffusion Process on a Dielectric Surface: Effects of Relative Humidity, J. Phys. Chem. C 125 (21) (2021) 11677–11686, http://dx.doi.org/10.1021/acs.jpcc.1c02272.

[30] S. Sadewasser, T. Glatzel (Eds.), Kelvin Probe Force Microscopy: From Single Charge Detection to Device Characterization, in: Springer Series in Surface Sciences, Springer International Publishing, 2018.

[31] C.Y. Ng, T.P. Chen, H.W. Lau, Y. Liu, M.S. Tse, O.K. Tan, V.S.W. Lim, Visualizing charge transport in silicon nanocrystals embedded in SiO2 films with electrostatic force microscopy, Appl. Phys. Lett. 85 (14) (2004) 2941–2943, http://dx.doi.org/10.1063/1.1801675.

[32] S.-D. Tzeng, S. Gwo, Charge trapping properties at silicon nitride/silicon oxide interface studied by variable-temperature electrostatic force microscopy, J. Appl. Phys. 100 (2) (2006) 023711, http://dx.doi.org/10.1063/1.2218025.

[33] Q. Hu, Q. Li, Z. Liu, N. Xue, H. Ren, M. Haddad, Surface Flashover Induced by Metal Contaminants Adhered to Tri-Post Epoxy Insulators under Superimposed Direct and Lightning Impulse Voltages, Polymers (Basel) 14 (7) (2022) 1374, http://dx.doi.org/10.3390/polym14071374.

[34] F.T. Xu, S.M. Thaler, C.A. Lopez, J.A. Barnard, A. Butera, J.L. Weston, Stable charge storage in granular thin films, Appl. Phys. Lett. 86 (7) (2005) 074105, http://dx.doi.org/10.1063/1.1868067.

[35] N. Amiour, Z. Ziari, S. Sahli, Traps energy distribution in Kapton HN polyimide films through surface potential decay model under humidity conditions, J. Electrostat. 109 (2021) 103551, http://dx.doi.org/10.1016/j.elstat.2021.103551.

[36] S.G.J. Mathijssen, M. Kemerink, A. Sharma, M. Cölle, P.A. Bobbert, R.a.J. Janssen, D.M. de Leeuw, Charge Trapping at the Dielectric of Organic Transistors Visualized in Real Time and Space, Adv. Mater. 20 (5) (2008) 975–979, http://dx.doi.org/10.1002/adma.200702688.

[37] U. Zaghloul, B. Bhushan, P. Pons, G.J. Papaioannou, F. Coccetti, R. Plana, On the influence of environment gases, relative humidity and gas purification on dielectric charging/discharging processes in electrostatically driven MEMS/NEMS devices, Nanotechnology 22 (3) (2011) 035705, http://dx.doi.org/10.1088/0957-4484/22/3/035705.

[38] A. Crisci, B. Gosse, J.-P. Gosse, V. Ollier-Duréault, Surface-potential decay due to surface conduction, Eur. Phys. J. AP 4 (1) (1998) 107–116, http://dx.doi.org/10.1051/epjap:1998249.

[39] D. Min, M. Cho, A.R. Khan, S. Li, Surface and volume charge transport properties of polyimide revealed by surface potential decay with genetic algorithm, IEEE Trans. Dielectr. Electr. Insul. 19 (2) (2012) 600–608, http://dx.doi.org/10.1109/TDEI.2012.6180255.

[40] A.E. Seaver, An Equation for Charge Decay Valid in Both Conductors and Insulators, 2008, arXiv:0801.4182 [Physics].

[41] J. Lambert, M. Saint-Jean, C. Guthmann, Contact electrification of high-K oxides studied by electrostatic force microscopy, J. Appl. Phys. 96 (12) (2004) 7361–7369, http://dx.doi.org/10.1063/1.1815386.

[42] R. Beyer, E. Beyreuther, J. von Borany, J. Weber, Charge storage in silicon-implanted silicondioxide layers examined by scanning probe microscopy, Thin Solid Films 513 (1) (2006) 159–165, http://dx.doi.org/10.1016/j.tsf.2006.02.002.

[43] J. Kindersberger, C. Lederle, Surface charge decay on insulators in air and sulfurhexafluorid - part I: simulation, IEEE Trans. Dielectr. Electr. Insul. 15 (4) (2008) 941–948, http://dx.doi.org/10.1109/tdei.2008.4591214.

[44] A.M. Somoza, E. Palacios-Lidón, Localized charges in thin films by Kelvin probe force microscopy: From single to multiple charges, Phys. Rev. B 101 (7) (2020) 075432, http://dx.doi.org/10.1103/PhysRevB.101.075432.

[45] N. Wadehra, N. Kumar, S. Mishra, R. Tomar, S. Chakraverty, Nano-electrical domain writing for oxide electronics, Appl. Surf. Sci. 509 (2020) 145214, http://dx.doi.org/10.1016/j.apsusc.2019.145214.

[46] J.F. Gonzalez, A.M. Somoza, E. Palacios-Lidón, Charge distribution from SKPM images, Phys. Chem. Chem. Phys. 19 (40) (2017) 27299–27304, http://dx.doi.org/10.1039/C7CP05401G.

[47] A. Sprenkels, W. Olthuis, P. Berveld, The application of silicon dioxide as an electret material, in: 6th International Symposium on Electrets,(ISE 6) Proceedings., 1988, pp. 165–169, http://dx.doi.org/10.1109/ISE.1988.38543.

[48] S.-H. Song, H.-H. Yang, C.-H. Han, S.-D. Ko, S.-H. Lee, J.-B. Yoon, Metal-oxide-semiconductor field effect transistor humidity sensor us- ing surface conductance, Appl. Phys. Lett. 100 (10) (2012) 101603, http://dx.doi.org/10.1063/1.3691936.

[49] M.F. Orihuela, A.M. Somoza, J. Colchero, M. Ortuño, E. Palacios-Lidón, Localized charge imaging with scanning Kelvin probe microscopy, Nanotechnology 28 (2) (2017) 025703, http://dx.doi.org/10.1088/1361-6528/28/2/025703.

[50] D. Ziegler, N. Naujoks, A. Stemmer, Feed-forward compensation of surface potential in atomic force microscopy, Rev. Sci. Instrum. 79 (6) (2008) 063704, http://dx.doi.org/10.1063/1.2947740.

[51] E. Palacios-Lidón, B. Pérez-García, J. Colchero, Enhancing dynamic scanning force microscopy in air: as close as possible, Nanotechnology 20 (8) (2009) 085707, http://dx.doi.org/10.1088/0957-4484/20/8/085707.

[52] J.K. Srivastava, M. Prasad, J.B. Wagner, Electrical Conductivity of Silicon Dioxide Thermally Grown on Silicon, J. Electrochem. Soc. 132 (4) (1985) 955–963, http://dx.doi.org/10.1149/1.2113993.